

**Ab initio variational transition state theory and
master equation study of the reaction
 $(\text{OH})_3\text{SiOCH}_2 + \text{CH}_3 \rightleftharpoons (\text{OH})_3\text{SiOC}_2\text{H}_5$**

Daniel Nurkowski¹, Stephen J. Klippenstein³, Yuri Georgievskii³, Marco
Verdicchio³, Ahren W. Jasper⁴, Jethro Akroyd¹, Sebastian Mosbach¹,
Markus Kraft^{1,2}

released: 22 October 2014

¹ Department of Chemical Engineering
and Biotechnology
University of Cambridge
New Museums Site
Pembroke Street
Cambridge, CB2 3RA
United Kingdom
E-mail: mk306@cam.ac.uk

² School of Chemical
and Biomedical Engineering
Nanyang Technological University
62 Nanyang Drive
Singapore 637459

³ Chemical Sciences and Engineering Division
Argonne National Laboratory
IL 60439, USA
E-mail: sjk@anl.gov

⁴ Sandia National Laboratories
Livermore, CA 94551-0969
E-mail: ajasper@sandia.gov

Preprint No. 147



Edited by

Computational Modelling Group
Department of Chemical Engineering and Biotechnology
University of Cambridge
New Museums Site
Pembroke Street
Cambridge CB2 3RA
United Kingdom

Fax: + 44 (0)1223 334796

E-Mail: c4e@cam.ac.uk

World Wide Web: <http://como.cheng.cam.ac.uk/>

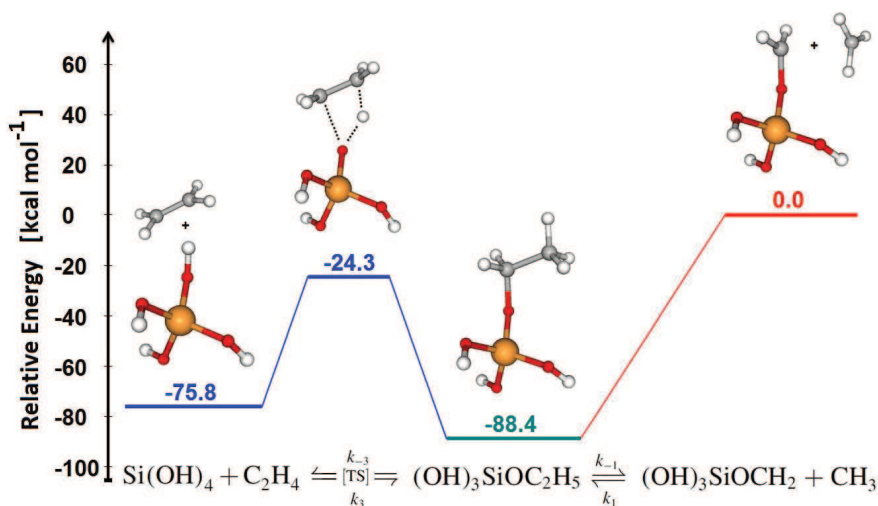


Highlights

- A detailed study of the kinetics of the title reaction is presented.
- Variable reaction coordinate transition state theory and master equation calculations are used to obtain rate constant coefficients at various pressures and temperatures.
- A comparison is made with an equivalent ethanol reaction computed at the same level of theory.

Abstract

In this paper we use variable reaction coordinate variational transition state theory (VRC-TST) to calculate the reaction rate constants for the two reactions, R1: $(\text{OH})_3\text{SiOCH}_2 + \text{CH}_3 \rightleftharpoons (\text{OH})_3\text{SiOC}_2\text{H}_5$, and R2: $\text{CH}_2\text{OH} + \text{CH}_3 \rightleftharpoons \text{C}_2\text{H}_5\text{OH}$. The first reaction is an important channel during the thermal decomposition of tetraethoxysilane (TEOS), and its rate coefficient is the main focus of this work. The second reaction is analogous to the first and is used as a basis for comparison. The interaction energies are obtained on-the-fly at the CASPT2(2e,2o)/cc-pVDZ level of theory. A one-dimensional correction to the sampled energies was introduced to account for the energetic effects of geometry relaxation along the reaction path. The computed, high-pressure rate coefficients were calculated to be, R1: $k_1 = 2.406 \times 10^{-10} T^{-0.301} \exp(-271.4/T) \text{ cm}^3 \text{ molecule}^{-1} \text{ s}^{-1}$ and R2: $k_2 = 1.316 \times 10^{-10} T^{-0.189} \exp(-256.5/T) \text{ cm}^3 \text{ molecule}^{-1} \text{ s}^{-1}$. These rates differ from each other by only 10-30% over the temperature range 300-2000 K. A comparison of the computed rates with experimental data shows good agreement and an improvement over previous results. The pressure dependency of the reaction R1 is explored by solving a master equation using helium as a bath gas. The results obtained show that the reaction is only weakly pressure dependent over the temperature range 300-1700 K, with the predicted rate constant being within 50% of its high-pressure limit at atmospheric pressure.



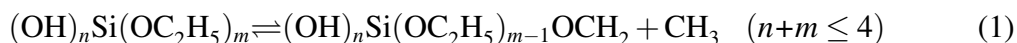
Contents

1	Introduction	3
2	Theory	5
2.1	Potential energy surface	5
2.2	Rate constant estimations	6
3	Results and discussion	9
3.1	Electronic structure calculations	9
3.2	Temperature dependence of R1 and R2 at the high pressure limit	10
3.3	Pressure dependence of k_{-1}	13
4	Conclusions	16
	References	17

1 Introduction

Tetraethoxysilane (TEOS) is an organosilicon material that is widely used as a precursor for the synthesis of silica nanoparticles. There is an increasing interest in studying the kinetics of TEOS because it offers a non-toxic and cost-effective manufacturing route [13, 16]. The most common production method is gas-to-particle conversion in flame reactors, where the precursor molecules decompose into various intermediates which eventually react to form solid nanoparticles [21, 48]. The focus of this paper is the kinetics of one of the main decomposition reactions in the TEOS system.

Two generally accepted decomposition routes of TEOS are 1,2-elimination of ethylene and C–C bond cleavage [4, 14]. Ethylene elimination channels decompose TEOS and its intermediates in a step-wise manner, eventually producing silicic acid $\text{Si}(\text{OH})_4$ as a final product. These reactions have an energy barrier which makes the prediction of their rate constants relatively straightforward. The C–C bond cleavage reactions generate silica and methyl radicals which may result in rapid chain decomposition processes [14]:



These reactions are barrier-less which poses some difficulties in estimating reliable rate coefficients. First of all, the molecules considered are quite large, making *ab initio* electronic structure calculations computationally expensive. Secondly, standard free-rotor and harmonic-oscillator approximations are inadequate to accurately describe the available number of states due to the loose nature of the transition state for which the typical distance between the two fragments is 2-4 Å [22]. A number of experimental and computational studies have been conducted to investigate the decomposition of TEOS, however, much uncertainty still exists in the kinetics of C–C bond cleavage reactions.

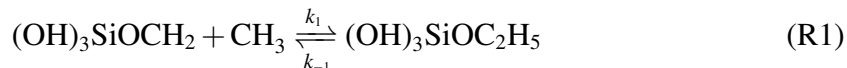
Herzler et al. [14] examined the decomposition of TEOS in a single-pulse shock tube over the temperature range of 1160-1285 K and at a pressure of 1.5 bar. The main products were found to be ethylene and ethanol, and a preliminary mechanism describing TEOS decomposition was proposed. The model parameters were found by fitting them against experimental observations and making assumptions about the Arrhenius coefficients for particular families of reactions. However, the reaction rate constant for the C–C bond cleavage channel was derived assuming that this is the only other decomposition route apart from 1,2-elimination of ethylene. An alternative decomposition route was proposed by Chu et al. [4]. Experiments were carried out in a heated wall reactor and a six-center decomposition mechanism producing equal amounts of ethylene, ethanol and silicate was suggested as the main initiating channel. However, this reaction was found to be in disagreement with Herzler’s [14] experimental observations. The importance of various reaction channels in TEOS decomposition was assessed by Ho and Melius [15] who used quantum chemistry to calculate thermodynamic properties of silica species. However, the computations are considered to be incomplete as they were only performed for key species rather than for all possible intermediates. Kraft and co-workers [34] made steps to address this problem by calculating thermodynamic properties for 180 silica species in the TEOS system. Equilibrium calculations were used to determine the most important intermediates and a heuristic model describing TEOS decomposition was proposed [42]. Subsequently, the model was coupled with a population balance equation code

[40, 41, 43–45, 50, 53] where it was assumed that silicic acid is the inception species. Computed particle size distributions at different temperatures were found to be consistent with experimental data [42].

In the most recent work of Nurkowski et al. [32], a detailed kinetic mechanism for the decomposition of TEOS was proposed based on the analogy with the decomposition of ethanol. A flux and sensitivity analysis of the proposed mechanism was shown to be consistent with the TEOS decomposition path proposed by Herzler [14]. *Ab initio* transition state theory was employed to calculate the reaction rate constants for the two most important channels: 1,2-elimination of ethylene and C–C bond cleavage. General transition state theory (TST) was used for the 1,2-elimination of ethylene (which has a barrier) and variational TST combined with Gorin model assumptions [35] was employed for the C–C bond cleavage (a barrier-less reaction). The computed rate constants were found to be similar to the equivalent ethanol reactions calculated at the same level of theory. The results from the ethanol system for reactions with barriers compared favourably with various modelling and experimental data, giving confidence that the chosen method was sufficient. However, the discrepancies between the experimental and modelling results for C–C bond cleavage in ethanol were significant, suggesting that a more accurate technique would be beneficial.

The purpose of this study is to obtain a more reliable rate coefficient for the C–C bond cleavage in the TEOS system and to explore the pressure dependence of this rate. To achieve this we employ variable reaction coordinate variational transition state theory (VRC-TST) [22–24] in combination with the master equation [30].

The current work is limited to the reaction (R1) involving silica species with only one ethoxy branch.



Firstly, this choice minimizes computational time and potential errors as this is the smallest silica molecule in the TEOS system. Secondly, it gives a good starting point for the prediction of the rate constants for the remaining channels. An analogous reaction from the ethanol system is also calculated at the same level of theory as a measure of accuracy and for comparison purposes.



The structure of this paper is as follows. Section 2.1 presents a description of the electronic structure methods used to obtain essential parameters of the reacting system. Section 2.2 explains how the high- and low- pressure rate coefficient are calculated. The results from the *ab initio* electronic structure computations are presented in section 3.1. The predicted high-pressure reaction rate constants for both R1 and R2 are shown in section 3.2, while information on the pressure dependence of reaction R1 can be found in section 3.3. Final conclusions are drawn in section 4.

2 Theory

2.1 Potential energy surface

The internal geometries, vibrational frequencies and hindered rotor potential energies for the reactants and products were computed with the hybrid density functional B97-1 method [2] using the 6-311+G(d,p) basis set [26] implemented in the Gaussian09 software package [9].

The interaction potential of the two reacting radicals, as a function of their separation and relative orientation, was obtained with the direct CASPT2 [1] method. The calculations were performed with a double- ζ basis set (cc-pVDZ) [6] and a two electron, two orbital active space. The internal structures of the fragments were kept fixed at their equilibrium geometries.

In order to account for the energetic effects of the geometry relaxation of the rigid fragments, a one-dimensional, orientation-independent, correction term was added to the CASPT2 potential energy. The correction was computed as the difference between energies obtained from the geometry optimisation of the fragment-fragment complex under two specific constraints. The first calculation optimised the structure at a given separation while varying all coordinates except the defined C–C distance (so relaxing the structure of each fragment). The second calculation optimised the transitional coordinates of the fragments whilst keeping the C–C distance constant and treating the fragments as rigid structures. All CASPT2 calculations were performed using the MOLPRO software package [52].

The C–C bond dissociation energy was obtained by employing a Gaussian-G2 method [5], which approximates restricted coupled-cluster energies with perturbative inclusion of the triplet contribution, RCCSD(T) [39], on a 6-311+G(3df,2p) basis set. The formula used in the computations is as follows [5, 38]

$$\begin{aligned} E(\text{G2}) = & E[\text{MP4}/6\text{-}311\text{+G}(\text{d,p})] \\ & + E[\text{MP4}/6\text{-}311\text{G}(2\text{df})] \\ & + E[\text{QCISD}(\text{T})/6\text{-}311\text{G}(\text{d,p})] \\ & - 2E[\text{MP4}/6\text{-}311\text{G}(\text{d,p})] \\ & + E[\text{MP2}/6\text{-}311\text{G}(\text{d,p})] - E[\text{MP2}/6\text{-}311\text{+G}(\text{d,p})] \\ & + E[\text{MP2}/6\text{-}311\text{+G}(3\text{df},2\text{p})] - E[\text{MP2}/6\text{-}311\text{G}(2\text{df},\text{p})] \\ & + 1.14n_{\text{pair}} - 5.95n_{\beta} - 0.19n_{\alpha} + \text{ZPE}[\text{HF}/6\text{-}31\text{G}(\text{d}) \times 0.893] \end{aligned} \quad (2)$$

where n_{pair} is the number of valence electron pairs and n_{α} and n_{β} are the number of alpha and beta electrons respectively. The zero point energy within the G2 method was calculated by using scaled vibrational frequencies (scaling factor of 0.893) taken from the HF/6-31G(d) model.

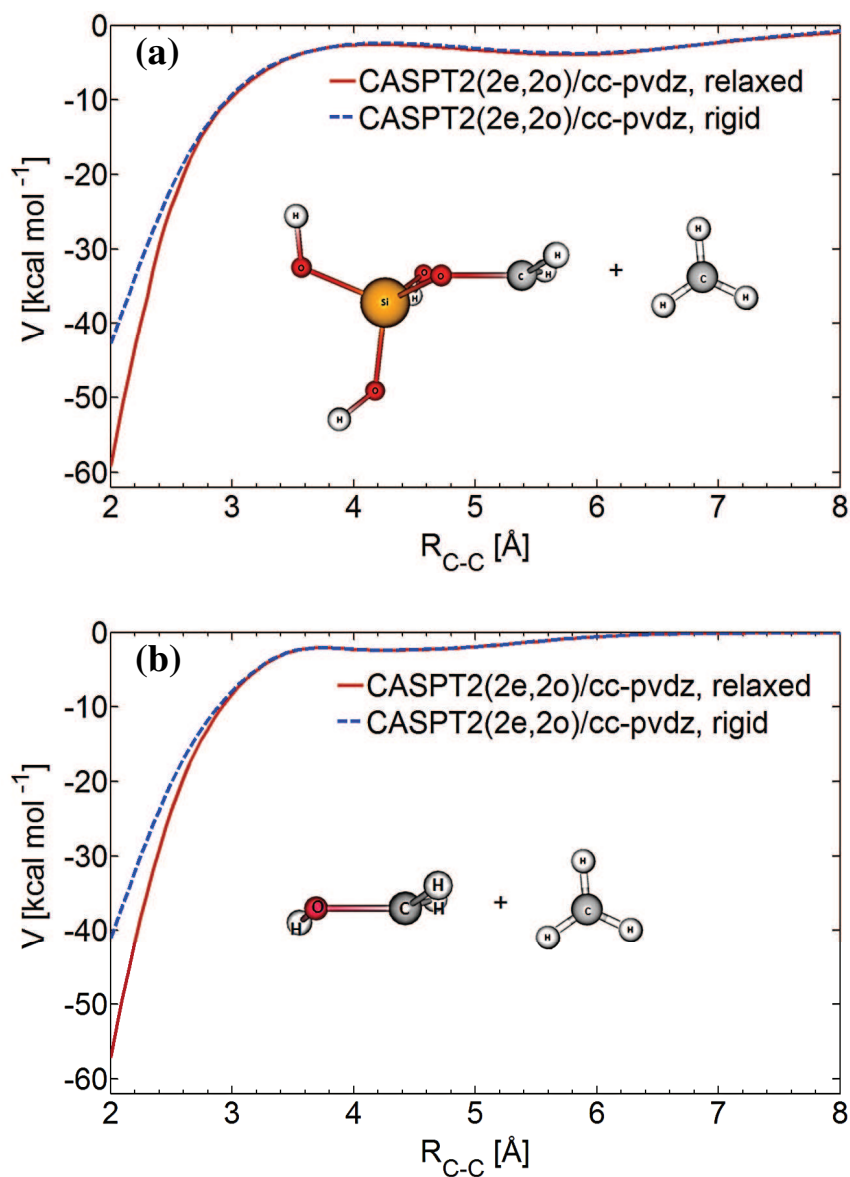


Figure 1: Comparison of the interaction potential energy curves from calculations in which the fragments' internal geometries were allowed to relax (dashed lines) or were held rigid (solid lines). All computations were performed at the CASPT2(2e,2o)/cc-pVDZ level.

2.2 Rate constant estimations

High-pressure limit rate constants. The high-pressure rate constants k_1 and k_2 for the barrier-less association of $(OH)_3SiOCH_2 + CH_3$ and $CH_2OH + CH_3$ radicals were estimated using VRC-TST [11]. Detailed descriptions of this method have been given elsewhere [10, 11, 23–25]. Thus, only the most important aspects are described here.

The reaction rate constant is computed according to a variational principle where the

optimal dividing surface is obtained through the minimization of the reactive flux. The reactive flux or available number of states, N^\ddagger , is calculated under the assumption of separability of the modes of motion in a reacting system into the conserved and transitional modes [11]. The number of states for the conserved modes is evaluated quantum mechanically (through a direct counting algorithm [3, 49]) whereas the number of states for the transitional modes involves classical phase space integrals [24]. Definition of the transition state dividing surfaces in VRC-TST is expressed in terms of a fixed distance between pivot points associated with the reacting fragments [10]. This allows the reaction coordinate to be more flexible and thus better describes the system at a given separation. The rate constant is finally computed by optimising both the position and relative separation of the pivot points.

In this paper, two different definitions of the reaction coordinate were used depending on the relative separation of fragments. For large interfragment distances (8-20 au), the pivot points were located at the mass centers of the corresponding molecules (a center of mass reaction coordinate). This was motivated by the fact that for large separations the motion of the entire system can be thought of as only a weak perturbation of the separate fragments. At smaller separations (4-7.5 au) the motion of the system is better understood as a perturbation of the molecular complex. Therefore, the pivot points should be placed close to the two atoms whose bond is going to break (a bond-length reaction coordinate [22]). In case of the $(\text{OH})_3\text{Si}(\text{OCH}_2)$ and CH_2OH the pivot points were located at the C atoms, whereas in case of the CH_3 the pivot points were placed along the C_3 symmetry axis at six possible displacements $\pm(0.01, 0.5, 1.0 \text{ au})$ with respect to the carbon atom.

Final calculations were done at the energy, E , and angular momentum, J , resolved level where the reactive flux, N_{EJ}^\ddagger , was minimised by finding the optimal dividing surface for each (E, J) pair (for energy equal or less than E and angular momentum quantum number equal to J). Optimization of the surface was performed at evenly spaced grid points with a spacing of 0.5 au for the small separations and at 8, 9, 10, 12, 14, 16, 18, 20 au for the large separations.

Pressure-dependent rate constants. The pressure dependence of reaction R1 was explored with master equation simulations [29–31]. At this point it became necessary to incorporate an additional reaction into the model. The reason for this is that in addition to the reaction R1, the molecule $(\text{OH})_3\text{SiOC}_2\text{H}_5$ can also dissociate via an ethylene elimination channel:



The reaction R3 has a tight transition state that is lower in energy than the endothermicity of the reaction R1. The dissociation via the lower energy channel changes the reactive distribution for the excited channel, and so must be considered when calculating the rate constant for reaction R1 at a particular pressure. The geometries, vibrational frequencies and energies of the stable species and the transition state in R3 were obtained using the methods described in section 2.1. An additional Eckart tunneling correction [7, 20] was included in the computations due to the high value of the imaginary frequency (1695 cm^{-1}) of the tight transition state. For the chosen range of the temperatures that reaction R3 was fitted to, the correction term ranges from a factor of 3 to a factor of 1.06.

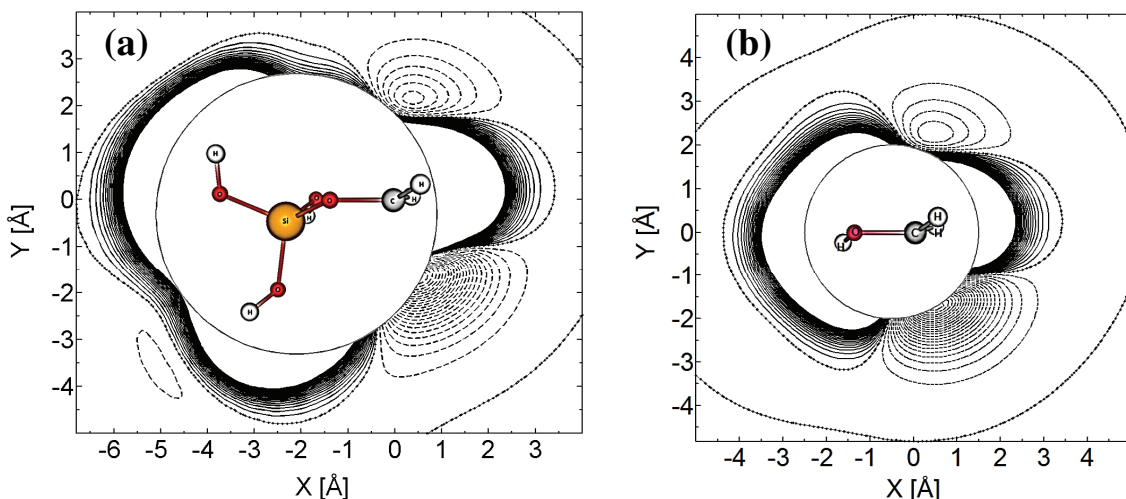


Figure 2: *Two dimensional contour plots of the CASPT2(2e,2o)/cc-pVDZ interaction potential for (a) $(\text{OH})_3\text{SiOCH}_2 + \text{CH}_3$ and (b) $\text{CH}_2\text{OH} + \text{CH}_3$. The plotting plane in both figures includes the central carbon atom and oxygen atom to the left. The plane bisects the angle between the two hydrogens to the right of the C atom. The plane of the approaching CH_3 is perpendicular to the plotting plane with the angle between the central carbon atom and one of the CH bonds in the methyl radical being fixed at 90° . The solid and dashed contour lines depict repulsive and attractive energies respectively. The contour increment is 1.0 kcal/mole. A zero energy contour is shown by the solid contour line with dot markers. The circle in the middle of each plot covers an irrelevant unplotted part of the potential energy surface.*

The density of states of the stable species and the number of states of the tight transition state in reaction R3 were evaluated on the basis of rigid-rotor harmonic-oscillator assumptions. The one exception from this rule was the treatment of a hindered CH_3 rotor in the $(\text{OH})_3\text{SiOC}_2\text{H}_5$ molecule that was described according to Pitzer-Gwinn approximation [36, 37]. The number of states of the loose transition state in reaction R1 was computed under the assumption of the separability of the modes of motion into conserved and transitional modes. The density of states of the conserved modes (the vibrational modes of each of the separate fragments) was evaluated at the harmonic-oscillator level. The number of states of the transitional modes (the rotational modes of the two individual fragments and the orbital motion) was computed via phase-space integrals. The final number of states was then obtained by convoluting the former with the latter.

The collision frequency, ω , was approximated by employing a Lennard-Jones (LJ) model. The LJ parameters were computed for $(\text{OH})_3\text{SiOC}_2\text{H}_5$ with He as the bath gas using the one-dimensional minimisation approach implemented in the OneDMin software [18]. These computations were performed with an MP2/aug-cc-pVDZ potential and similar calculations have shown these methods to predict Lennard-Jones collision rates at an accuracy of $\pm 10\%$ [17].

The energy transfer probability was approximated by the exponential down model with

the temperature-dependent average energy transferred per collision parameter described by the following equation: $\langle \Delta E_{\text{down}} \rangle = \langle \Delta E_{\text{down}}^0 \rangle (T/300K)^{0.85}$. The value of the $\langle \Delta E_{\text{down}}^0 \rangle$ prefactor [12] was set to 400 cm^{-1} , which is a reasonable choice considering the size of the molecule and type of the collider (e.g., in our recent study of CxHy systems [19] similar sized systems were found to have values of about 350 cm^{-1}).

3 Results and discussion

3.1 Electronic structure calculations

The calculated one-dimensional interaction energies for both reactions R1 and R2 are depicted in **Figure 1**. The value of the relaxation correction term (the difference between the two curves) varies from 0.01 to 16 kcal/mol and is most significant for separations in the range 2-3 Å. The correction is essential for barrier-less reactions, where the distance between the fragments forming the transition state complex is typically in this range. Additionally, for both reactions, a small saddle-point can be noticed at around 4 Å. This is an effect of the dominant forces acting on the fragments changing from long-range van der Waals forces to short-range chemical bonding forces as the separation between the fragments decreases. This change is accompanied by the re-orientation of the fragments to a different minima; hence the presence of the saddle point.

Figure 2 shows part of the potential energy surface computed at the CASPT2 level for R1 and R2. Due to the high dimensionality of the system, the plots are restricted to a specific orientation of the fragments. In both cases, a plotting plane was spanned by a vector pointing from the central carbon atom towards the oxygen atom on its left and a vector bisecting an angle between the two hydrogens attached to the carbon atom on its right. The plane of the approaching CH₃ radical was kept perpendicular to the plotting plane with the additional restriction that the angle formed by the central carbon atom and one of the CH bonds in CH₃ is fixed at 90°. There are two possible CH₃ addition sites for both reactions. These are the areas with strongly attractive (negative) potential. The first site, which will be referred to as the front, is defined by the two hydrogens in the -OCH₂ group pointing away from the approaching CH₃. The second site, which will be referred to as the back, is defined by the same two hydrogens pointing towards the CH₃. A total rate constant is calculated as the sum of front and back additions. It has to be mentioned that there are also two possible ways for the CH₃ radical to approach the two addition sites of the -OCH₂ group. However, due to symmetry, the total contribution is readily obtained by evaluating the contribution for one approach and then multiplying that contribution by a degeneracy factor of two.

Table 1 presents the zero-point corrected total energies, E_0 , of each species involved in reactions R1, R2, and R3 obtained at different levels of theory. The corresponding C–C bond dissociation energies, D_0 , and activation energies, E_0^\ddagger , are also computed. It can be noticed that the performance of the B3LYP hybrid functional is quite poor, with around 8 kcal mol^{-1} difference compared to the G2 calculations, where the G2 is the most detailed of the methods used in this paper.

Table 1: Stationary point energies for reactions R1, R2 and R3.^a

Species / Reactions	G2 ^b	MP2 ^c	B97-1 ^c	B3LYP ^c
	E_0 (hartree)			
(OH) ₃ SiOC ₂ H ₅	-670.6723	-670.1964	-671.4811	-671.6524
(OH) ₃ SiOCH ₂	-630.7863	-630.3784	-631.5434	-631.7004
Si(OH) ₄	-592.2362	-591.8818	-592.9311	-593.0737
(OH) ₃ SiO...H...C ₂ H ₄	-670.5701	-670.0955	-671.3873	-671.5606
C ₂ H ₅ OH	-154.7645	-154.5638	-154.9587	-155.0153
CH ₂ OH	-114.8816	-114.7489	-115.0235	-115.0654
C ₂ H ₄	-78.4159	-78.2952	-78.5307	-78.5647
CH ₃	-39.7451	-39.6783	-39.8026	-39.8255
	D_0 (kcal mol ⁻¹) ^d			
(OH) ₃ SiOC ₂ H ₅ → (OH) ₃ SiOCH ₂ + CH ₃	88.4	87.6	84.8	79.3
C ₂ H ₅ OH → CH ₂ OH + CH ₃	86.5	85.7	83.2	78.0
	E_0^\ddagger (kcal mol ⁻¹) ^e			
(OH) ₃ SiOC ₂ H ₅ → Si(OH) ₄ + C ₂ H ₄	64.1	63.3	58.9	57.6

^a Zero point corrections are included throughout. Units are hartree and kcal mol⁻¹

^b Gaussian G2 method estimating RCCSD(T)/6-311+G(3df,2p) energies

^c MP2, B97-1, and B3LYP computations for the 6-311+G(d,p) basis set

^d The zero-point corrected bond dissociation energies at 0 K for the given channels

^e The zero-point corrected activation energies at 0 K for the given channels

The C–C bond dissociation energies, D_0 , of the ethanol reaction were compared with the high accuracy calculations reported by Sivaramakrishnan et al. [46], who report energies of 85.1 kcal mol⁻¹ calculated using the QCSID(T)/CBS level of theory and 85.33 kcal mol⁻¹ using the Active Thermochemical Tables method. In this particular case, the data in Table 1 shows that the MP2 estimations compare more favourably than the G2 predictions for the ethanol reaction. However, it was decided to use the G2 results for the rate constant calculations for both the silica and ethanol systems. This was motivated by the fact that in general the G2 technique is more accurate than the MP2 computations [8, 47], and there is no data available to say whether the above observation regarding the MP2 estimations will generalise to the silica reaction.

3.2 Temperature dependence of R1 and R2 at the high pressure limit

The present theoretical predictions of the high-pressure rate constants k_1 and k_2 are compared in Figure 3. The computed k_2 rate coefficients are additionally compared with the

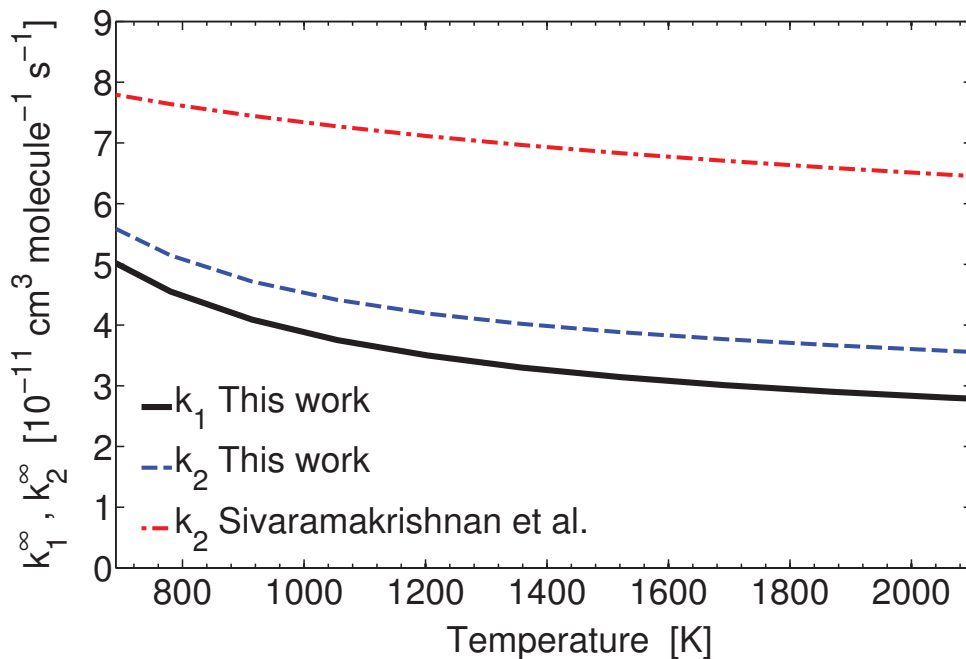


Figure 3: The theoretical predictions for the high-pressure association rate constants. Solid and dashed lines represent our results for the silica (k_1) and ethanol (k_2) reactions respectively.

related *ab initio* TST simulations from Sivaramakrishnan et al. [46].

As shown, the rate constants k_1 and k_2 estimated in this work are very similar to each other, with differences of the order 10-30% for the temperature range 800-2000 K. A reduction from the reaction rate coefficient of reaction R2 to R1 is expected due to the increased steric bulk of the Si group. However, this steric reduction is ameliorated to some extent by an increased long-range attraction as illustrated in Figure 2. The net effect is a modest reduction that may be within the error bars of the VRC-TST method [25]. Additionally, both association rate coefficients are predicted to have small negative temperature dependencies. They decrease by $\sim 40\%$ from 800 to 2000 K.

For k_2 , the predictions of Sivaramakrishnan et al. [46] are 45-70% higher than the current results over the studied temperature range. These differences arise from the use of a lower level of theory in this work because of the desire to look at the bigger Si system as compared to Sivaramakrishnan et al. [46] who only considered the ethanol system. The level of agreement with Sivaramakrishnan et al. [46] then gives some validation of the reduction in the level of theory used in this work.

Figure 4 illustrates the computed high-pressure rate constants in the dissociation direction (k_{-1} and k_{-2}). In Fig. 4 (a) the data for reaction R1 are compared to our previous Gorin Model predictions [32] and the experimentally derived rates of Herzler et al. [14]. Fig. 4 (b) depicts the results for reaction R2 contrasted with experimental and modelling studies from Li et al. [27], Park et al. [33], Marinov [28], Sivaramakrishnan et al. [46], and our previous Gorin Model predictions [32].

As expected, the Gorin Model calculations provide rates which are much higher (around

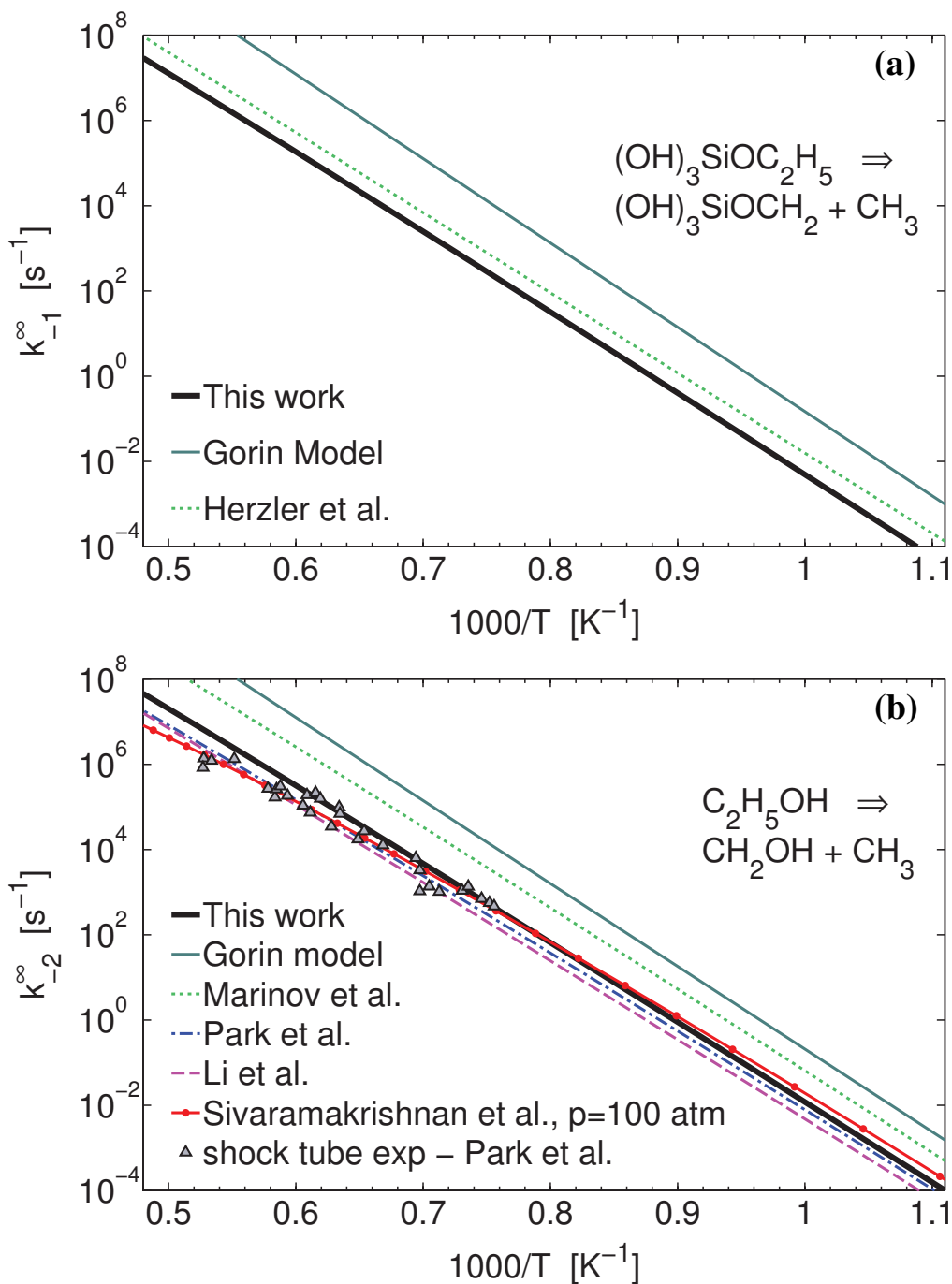


Figure 4: Arrhenius plots of the theoretical predictions for the high-pressure dissociation rate constants (a) k_{-1}^{∞} and (b) k_{-2}^{∞} compared with various experimental and modelling data.

one order of magnitude) than the current results for both R1 and R2. This supports the suggestion in our previous paper [32] that a more detailed calculation is needed for these reactions. The superiority of the VRC-TST technique over the Gorin model approach is evident and lies in the proper treatment of the transitional mode contribution to the

transition state number of states N_{EJ}^\ddagger . Within the VRC-TST approach the transitional mode contribution to N_{EJ}^\ddagger is computed through classical phase space integrals, resulting in an accurate description of the mode-mode couplings and angular momentum conservation.

Further examination of Figure 4 (a) indicates that the rate constant provided by Herzler et al. [14] is a factor of 5 higher than our predictions. This difference is not surprising given that Herzler’s rate constant was derived from a fitting of model predictions to experimental data.

Figure 4 (b) is presented for the assessment of accuracy of the chosen method. It shows data for the ethanol reaction R2 compared to various modelling and experimental results. The newly predicted rate constants are about a factor of 1.5-2 higher than the theoretical results of Park et al. [33] and the modelling values from Li et al. [27]. However, Park et al. [33] employed a simple Morse function as an interaction potential, whereas Li et al. [27] derived this rate from the equilibrium constant and an empirical high-pressure rate coefficient for the reverse reaction taken from Tsang [51]. Thus, the observed discrepancies are not surprising. Overall, a good agreement with the experimental measurements of Park et al. [33] is observed, where the current computations only slightly overestimate the experimentally determined rate coefficients. The differences slowly increase with increasing temperature. Unfortunately, the uncertainties of the Park’s measurements are not provided.

Marinov’s estimates [28] were obtained by combining the Gorin Model with parameter fitting to match shock-tube experimental data for which the current reaction was found to be sensitive. Not surprisingly, his results are closer to our prior Gorin Model computations than to the current VRC-TST predictions.

The results of Sivaramakrishnan et al. [46] were obtained from the experimental measurements of ethanol dissociation in a shock tube combined with *ab initio* transition state theory-based master equation simulations. The rate coefficients were computed up to a pressure of 100 atm, which was then used for the comparison to our high-pressure limit predictions. Based on the curvature of the line representing the Sivaramakrishnan et al. [46] data, it can be inferred that their rate coefficients are in the fall-off regime for temperatures above 1100 K. This explains the differences between the results in this paper and those of Sivaramakrishnan et al. [46] above 1100 K. A meaningful comparison can still be made for temperatures in the range 800-1100 K. It can then be noticed that the computations performed in the present work are within a factor of 2 of the Sivaramakrishnan et al. [46] calculations. The observed discrepancies can again be explained by the differences in the level of theory used in modelling these reactions. In the present work a level of theory was limited by the bigger Si system. Nevertheless, the results obtained for ethanol indicate that the resulting accuracy is satisfactory.

3.3 Pressure dependence of k_{-1}

Pressure effects on reaction R1 were explored by solving the master equation. **Figure 5** presents the rate constants k_{-1} (in the dissociation direction) obtained for different pressures and temperatures. The plotted fall-off curves are normalised by the corresponding high-pressure limit rate constants at a particular temperature.

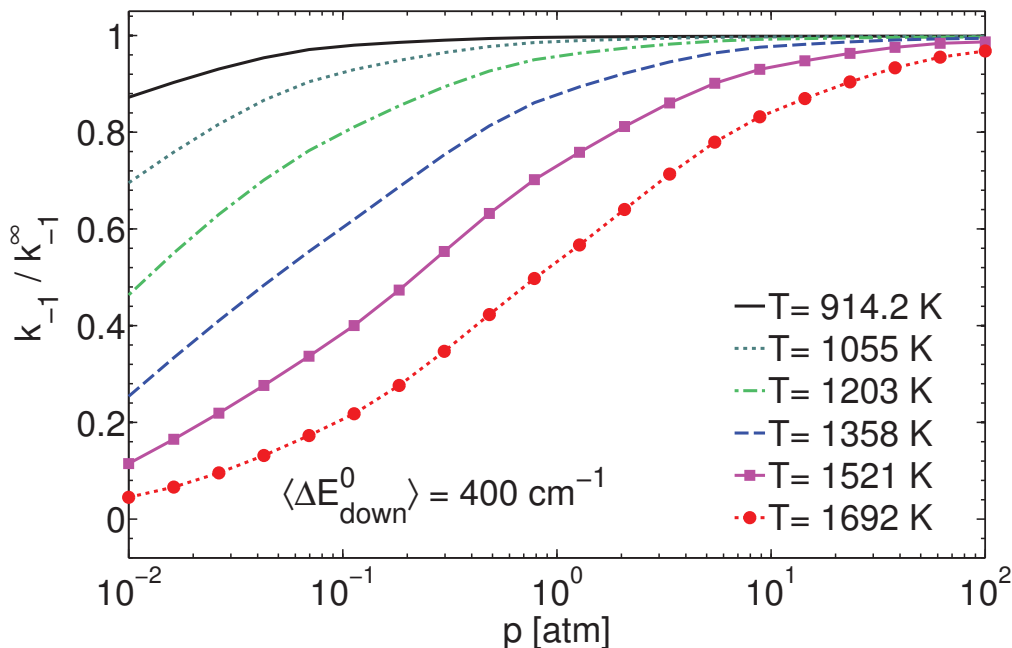


Figure 5: Fall off curves for the reaction $(\text{OH})_3\text{SiOC}_2\text{H}_5 \rightleftharpoons (\text{OH})_3\text{SiOCH}_2 + \text{CH}_3$ relative to its high-pressure limit.

Typically, master equation calculations are tuned to reproduce experimental data. The parameters that could vary are, for example, the pre-factor in $\langle \Delta E_{\text{down}} \rangle$ equation (if this model is used) or the height of the dissociation energy barrier, D_0 , (within the error bars of the method that was used to obtain it). Unfortunately, no experimental measurements exist for the investigated reaction. Therefore, it was decided to simply present the results for a fixed $\langle \Delta E_{\text{down}}^0 \rangle$ of 400 cm^{-1} and for the estimated barrier height. We expect that the uncertainty in each of these parameters may contribute about a factor of two to the uncertainty in the predicted rate constant.

It can be seen from Fig. 5 that the reaction R1 has a fairly weak dependence on pressure. The rate constant k_{-1} attains more than 90% of its high-pressure limit value, k_{-1}^∞ , at atmospheric pressure and temperatures up to 1358 K. At temperatures near 1700 K and atmospheric pressure k_{-1} is still within 50% of k_{-1}^∞ . This behaviour is not surprising, because as the molecule gets larger the rate of dissociation at a given energy decreases. The decreased rate of dissociation implies more collisions before dissociation and so a more thermalized (i.e., closer to the high pressure limit) dissociative distribution. Therefore, a weaker pressure-dependency is expected for larger intermediates. It should be noted that the $(\text{OH})_3\text{SiOC}_2\text{H}_5$ molecule is the smallest silica species able to undergo a C–C bond cleavage reaction.

Table 2 shows the temperature and pressure dependent rate constants for reaction R1 in modified Arrhenius form. In order to obtain an accurate fit for k_{-1} it was decided to split the temperature range into the two shown regimes. The high-pressure limit rate coefficients for reactions R2, R3 and the Lennard-Jones parameters used in the master equation calculations are also reported in Table 2.

Table 2: Predicted rate constants at different temperatures, T , and pressures, P , in the form of the modified Arrhenius equations $k = AT^n \exp(E_0/T)$ for reaction R1, R2 and R3. The Lennard-Jones coefficients used in the pressure-dependency computations are also reported.^a

Reaction		$(\text{OH})_3\text{SiOCH}_2 + \text{CH}_3 \xrightleftharpoons[k_{-1}]{k_1} (\text{OH})_3\text{SiOC}_2\text{H}_5$					
300 - 2000 K							
	P	A	n	E_0			
k_1	∞	2.406×10^{-10}	-0.301	-271.4			
300 - 800 K							
	P	A	n	E_0	800 - 2000 K		
	0.01	3.892×10^{19}	-0.763	45144	1.207×10^{86}	-20.436	62475
	0.1	1.066×10^{19}	-0.579	45071	4.360×10^{70}	-15.714	59275
	1	9.122×10^{18}	-0.556	45062	2.908×10^{51}	-10.052	54226
k_{-1}	10	8.975×10^{18}	-0.554	45061	3.637×10^{35}	-5.420	49675
	100	8.961×10^{18}	-0.554	45061	1.192×10^{27}	-2.965	47151
	∞	8.857×10^{18}	-0.552	45060	1.351×10^{24}	-2.114	46263
Reaction		$\text{CH}_2\text{OH} + \text{CH}_3 \xrightleftharpoons[k_{-2}]{k_2} \text{C}_2\text{H}_5\text{OH}$					
300 - 2000 K							
	P	A	n	E_0			
k_2	∞	1.316×10^{-10}	-0.189	-256.5			
k_{-2}	∞	3.989×10^{21}	-1.390	44599			
Reaction		$\text{Si}(\text{OH})_4 + \text{C}_2\text{H}_4 \xrightleftharpoons[k_{-3}]{k_3} (\text{OH})_3\text{SiOC}_2\text{H}_5$					
500 - 2000 K							
	P	A	n	E_0			
k_3	∞	6.642×10^{-11}	-0.141	-435			
k_{-3}	∞	2.527×10^7	1.875	30969			
Lennard-Jones Parameters							
$(\text{OH})_3\text{SiOC}_2\text{H}_5\text{-He}^b$		$\varepsilon = 53.22 \text{ cm}^{-1}$		$\sigma = 4.319 \text{ \AA}$			

^a Units are atmospheres, cm^3 , seconds, kelvins and molecules.

^b This work, computed for the MP2/aug-cc-pvdz potential, see text

4 Conclusions

The kinetics of the C–C bond cleavage in the $(\text{OH})_3\text{SiOC}_2\text{H}_5$ molecule have been investigated by VRC-TST combined with multireference CASPT2(2e,2o)/cc-pVDZ electronic structure calculations over a wide range of temperatures. The analogous ethanol decomposition reaction was studied at the same level of theory for comparison and assessment of accuracy. The results show that the current technique provides rate constant estimates with much higher accuracy compared to a simple Gorin Model. Additionally, it was shown that for this level of theory, a strong similarity exists between the high-pressure limit rate constants for both systems, with differences of only 10-30%.

The pressure dependence of reaction R1 was explored by solving the master equation while employing the VRC-TST data for the transition state number of states. The predicted fall-off curves for a wide range of different pressures show that the pressure dependency is rather weak. At atmospheric pressure and combustion relevant temperatures (1000-1700 K) the computed rate constant is still within 50-100% of its high-pressure limit. Even weaker dependence is expected for larger silica species such as TEOS. All computed forward and reverse rate constants for reaction R1 were fitted to modified Arrhenius expressions.

Acknowledgements

The work at Argonne was supported by the US Department of Energy, Office of Basic Energy Sciences, Division of Chemical Sciences, Geosciences, and Biosciences, under Contract No. DE-AC02-06CH11357. This project is partly funded by the National Research Foundation (NRF), Prime Minister's Office, Singapore under its Campus for Research Excellence and Technological Enterprise (CREATE) programme.

References

- [1] K. Andersson, P. Å. Malmqvist, and B. O. Roos. Second-order perturbation theory with a complete active space self-consistent field reference function. *Journal of Chemical Physics*, 96(2):1218–1226, 1992. doi:10.1063/1.462209.
- [2] A. D. Becke. Density-functional thermochemistry. III. The role of exact exchange. *Journal of Chemical Physics*, 98(7):5648–5651, 1993. doi:10.1063/1.464913.
- [3] T. Beyer and D. F. Swinehart. Algorithm 448: Number of multiply-restricted partitions. *Communications of the ACM*, 16(6):379–379, 1973. doi:10.1145/362248.362275.
- [4] J. C. S. Chu, J. Breslin, N. Wang, and M. C. Lin. Relative stabilities of tetramethyl orthosilicate and tetraethylorthosilicate in the gas phase. *Materials Letters*, 12:179–184, 1991. doi:10.1016/0167-577X(91)90170-B.
- [5] L. A. Curtiss, K. Raghavachari, G. W. Trucks, and J. A. Pople. Gaussian-2 theory for molecular energies of first- and second-row compounds. *Journal of Chemical Physics*, 94:7221–7230, 1991. doi:10.1063/1.460205.
- [6] T. H. Dunning. Gaussian basis sets for use in correlated molecular calculations. I. The atoms boron through neon and hydrogen. *Journal of Chemical Physics*, 90(2):1007–1023, 1989. doi:10.1063/1.456153.
- [7] C. Eckart. The Penetration of a Potential Barrier by Electrons. *Physical Review*, 36:878–892, 1930. doi:10.1103/PhysRev.36.878.
- [8] J. B. Foresman and Æ. Frish. *Exploring Chemistry with Electronic Structure Methods*. Gaussian; 2 edition, 1996. ISBN 978-0963676931.
- [9] M. J. Frisch, G. W. Trucks, H. B. Schlegel, G. E. Scuseria, Robb, et al. Gaussian09 Revision D.01, 2009. Gaussian Inc. Wallingford CT 2009.
- [10] Y. Georgievskii and S. J. Klippenstein. Transition State Theory for Multichannel Addition Reactions: Multifaceted Dividing Surfaces. *Journal of Physical Chemistry A*, 107(46):9776–9781, 2003. doi:10.1021/jp034564b.
- [11] Y. Georgievskii and S. J. Klippenstein. Variable reaction coordinate transition state theory: Analytic results and application to the $C_2H_3 + H \rightarrow C_2H_4$ reaction. *Journal of Physical Chemistry A*, 110(36):10528–10544, 2006. doi:10.1021/jp062693x.
- [12] R. G. Gilbert. Theory of collisional energy transfer of highly excited molecules. *International Reviews In Physical Chemistry*, 10(3):319–347, 1991. doi:10.1080/01442359109353261.
- [13] C. Hankwon, J. H. Park, and H. D. Jang. Flame synthesis of silica nanoparticles by adopting two-fluid nozzle spray. *Colloids and Surfaces A: Physicochemical and Engineering Aspects*, 313-314:140–144, 2008. doi:10.1016/j.colsurfa.2007.04.083.

- [14] J. Herzler, J. A. Manion, and W. Tsang. Single-pulse shock tube study of the decomposition of tetraethoxysilane and related compounds. *Journal of Physical Chemistry A*, 101:5500–5508, 1997. doi:10.1021/jp9706543.
- [15] P. Ho and C. F. Melius. Theoretical study of the thermochemistry of molecules in the Si-O-H-C system. *Journal of Physical Chemistry*, 99:2166–2176, 1995. doi:10.1021/j100007a056.
- [16] H. D. Jang. Generation of silica nanoparticles from tetraethylorthosilicate (TEOS) vapor in a diffusion flame. *Aerosol Science and Technology*, 30(5):477–488, 1999. doi:10.1080/027868299304516.
- [17] A. W. Jasper and J. A. Miller. Theoretical Unimolecular Kinetics for $\text{CH}_4 + \text{M} \rightleftharpoons \text{CH}_3 + \text{H} + \text{M}$ in Eight Baths, $\text{M} = \text{He}, \text{Ne}, \text{Ar}, \text{Kr}, \text{H}_2, \text{N}_2, \text{CO},$ and CH_4 . *Journal of Physical Chemistry A*, 115(24):6438–6455, 2011. doi:10.1021/jp200048n.
- [18] A. W. Jasper and J. A. Miller. Lennard-Jones parameters for combustion and chemical kinetics modeling from full-dimensional intermolecular potentials. *Combustion and Flame*, 161(1):101–110, 2014. doi:10.1016/j.combustflame.2013.08.004.
- [19] A. W. Jasper, C. M. Oana, and J. A. Miller. “Third-body” collision efficiencies for combustion modeling: Hydrocarbons in atomic and diatomic baths. *Proceedings of the Combustion Institute*, 34, 2014. doi:10.1016/j.proci.2014.05.105. online.
- [20] H. S. Johnston and J. Heicklen. Tunnelling corrections for unsymmetrical Eckart potential energy barriers. *Journal of Physical Chemistry*, 66(3):532–533, 1962. doi:10.1021/j100809a040.
- [21] H. K. Kammler, L. Mädler, and S. E. Pratsinis. Flame Synthesis of Nanoparticles. *Chemical Engineering & Technology*, 24(6):583–596, 2001.
- [22] S. J. Klippenstein. A bond length reaction coordinate for unimolecular reactions. II. Microcanonical and canonical implementations with application to the dissociation of NCNO. *Journal of Chemical Physics*, 94(10):6469–6482, 1991. doi:10.1063/1.460276.
- [23] S. J. Klippenstein. Variational optimizations in the Rice–Ramsperger–Kassel–Marcus theory calculations for unimolecular dissociations with no reverse barrier. *Journal of Chemical Physics*, 96(1):367–371, 1992. doi:10.1063/1.462472.
- [24] S. J. Klippenstein. An Efficient Procedure for Evaluating the Number of Available States within a Variably Defined Reaction Coordinate Framework. *Journal of Physical Chemistry*, 98(44):11459–11464, 1994. doi:10.1021/j100095a032.
- [25] S. J. Klippenstein, Y. Georgievskii, and L. B. Harding. Predictive theory for the combination kinetics of two alkyl radicals. *Journal of Physical Chemistry Chemical Physics*, 8:1133–1147, 2006. doi:10.1039/B515914H.

- [26] R. Krishnan, J. S. Binkley, R. Seeger, and J. A. Pople. Selfconsistent molecular orbital methods. XX. A basis set for correlated wave functions. *Journal of Chemical Physics*, 72(1):650–654, 1980. doi:10.1063/1.438955.
- [27] J. Li, A. Kazakov, and F. L. Dryer. Experimental and Numerical Studies of Ethanol Decomposition Reactions. *Journal of Physical Chemistry A*, 108(38):7671–7680, 2004. doi:10.1021/jp0480302.
- [28] N. M. Marinov. A detailed chemical kinetic model for high temperature ethanol oxidation. *International Journal of Chemical Kinetics*, 31(3):183–220, 1999.
- [29] J. A. Miller and S. J. Klippenstein. Theoretical Considerations in the NH_2 + NO Reaction. *Journal of Physical Chemistry A*, 104(10):2061–2069, 2000. doi:10.1021/jp992836y.
- [30] J. A. Miller and S. J. Klippenstein. Master Equation Methods in Gas Phase Chemical Kinetics. *Journal of Chemical Physics*, 118(12):5442–5455, 2002. doi:10.1063/1.1539035.
- [31] J. A. Miller, S. J. Klippenstein, and S. H. Robertson. A Theoretical Analysis of the Reaction between Vinyl and Acetylene: Quantum Chemistry and Solution of the Master Equation. *Journal of Physical Chemistry A*, 104(32):7525–7536, 2000. doi:10.1021/jp000687+.
- [32] D. Nurkowski, P. Buerger, J. Akroyd, and M. Kraft. A detailed kinetic study of the thermal decomposition of tetraethoxysilane. *Proceedings of the Combustion Institute*, 2014. doi:10.1016/j.proci.2014.06.093. online.
- [33] J. Park, R. S. Zhu, and M. C. Lin. Thermal decomposition of ethanol. i. Ab initio molecular orbital/Rice-Ramsperger-Kassel-Marcus prediction of rate constant and product branching ratios. *Journal of Chemical Physics*, 117, 2002. doi:10.1063/1.1490601.
- [34] W. Phadungsukanan, S. Shekar, R. Shirley, M. Sander, R. H. West, and M. Kraft. First-principles thermochemistry for silicon species in the decomposition of tetraethoxysilane. *Journal of Physical Chemistry A*, 113:9041–9049, 2009. doi:10.1021/jp905494s.
- [35] I. G. Pitt, R. G. Gilbert, and K. R. Ryan. Extended Gorin Model for Radical–Radical Recombination Reactions. *Journal of Physical Chemistry*, 99:239–247, 1995. doi:10.1021/j100001a037.
- [36] K. S. Pitzer and W. D. Gwinn. Energy Levels and Thermodynamic Functions for Molecules with Internal Rotation I. Rigid Frame with Attached Tops. *Journal of Chemical Physics*, 10:428–440, 1942. doi:10.1063/1.1723744.
- [37] K. S. Pitzer and W. D. Gwinn. Energy Levels and Thermodynamic Functions for Molecules with Internal Rotation: II. Unsymmetrical Tops Attached to a Rigid Frame. *Journal of Chemical Physics*, 14:239–243, 1946. doi:10.1063/1.1932193.

- [38] J. A. Pople, M. Head-Gordon, D. J. Fox, K. Raghavachari, and L. A. Curtiss. Gaussian-1 theory: A general procedure for prediction of molecular energies. *Journal of Chemical Physics*, 90:5622–5629, 1989. doi:10.1063/1.456415.
- [39] K. Raghavachari, G. W. Trucks, J. A. Pople, and M. Head-Gordon. A fifth-order perturbation comparison of electron correlation theories. *Chemical Physics Letters*, 157(6):479–483, 1989. doi:10.1016/S0009-2614(89)87395-6.
- [40] M. Sander, R. H. West, M. S. Celnik, and M. Kraft. A Detailed Model for the Sintering of Polydispersed Nanoparticle Agglomerates. *Aerosol Science and Technology*, 43(10):978–989, 2009. doi:10.1080/02786820903092416.
- [41] S. Shekar, W. J. Menz, A. J. Smith, M. Kraft, and W. Wagner. On a multivariate population balance model to describe the structure and composition of silica nanoparticles. *Computers and Chemical Engineering*, 43(10):130–147, 2012. doi:10.1016/j.compchemeng.2012.04.010.
- [42] S. Shekar, M. Sander, R. C. Riehl, A. J. Smith, A. Braumann, and M. Kraft. Modelling the flame synthesis of silica nanoparticles from tetraethoxysilane. *Chemical Engineering Science*, 70(5):54–66, 2012. doi:10.1016/j.ces.2011.06.010.
- [43] S. Shekar, A. J. Smith, W. J. Menz, M. Sander, and M. Kraft. A multidimensional population balance model to describe the aerosol synthesis of silica nanoparticles. *Journal of Aerosol Science*, 44:83–98, 2012. doi:10.1016/j.jaerosci.2011.09.004.
- [44] R. Shirley, Y. Liu, T. S. Totton, R. H. West, and M. Kraft. First-Principles Thermochemistry for the Combustion of a TiCl₄ and AlCl₃ Mixture. *Journal of Physical Chemistry A*, 113(49):13790–13796, 2009. doi:10.1021/jp905244w.
- [45] R. Shirley, J. Akroyd, L. A. Miller, O. R. Inderwildi, U. Riedel, and M. Kraft. Theoretical insights into the surface growth of rutile TiO₂. *Combustion and Flame*, 156(10):1868–1876, 2011. doi:10.1016/j.combustflame.2011.06.007.
- [46] R. Sivaramakrishnan, M. C. Su, J. V. Michael, S. J. Klippenstein, L. B. Harding, and B. Ruscic. Rate Constants for the Thermal Decomposition of Ethanol and Its Bimolecular Reactions with OH and D: Reflected Shock Tube and Theoretical Studies. *Journal of Physical Chemistry A*, 114(35):9425–9439, 2010. doi:10.1021/jp104759d.
- [47] B. J. Smith and L. Radom. Gas-phase acidities: a comparison of density functional, MP2, MP4, F4, G2(MP2, SVP), G2(MP2) and G2 procedures. *Chemical Physics Letters*, 245(1):123–128, 1995. doi:10.1016/0009-2614(95)00988-G.
- [48] J. Smolik and P. Moravec. Gas phase synthesis of fine silica particles by oxidation of tetraethylorthosilicate vapour. *Journal of Materials Science Letters*, 14(6):387–389, 1995. doi:10.1007/BF00274548.
- [49] S. E. Stein and B. S. Rabinovitch. Accurate evaluation of internal energy level sums and densities including anharmonic oscillators and hindered rotors. *The Journal of Chemical Physics*, 58(6):2438–2445, 1973. doi:10.1063/1.1679522.

- [50] T. S. Totton, R. Shirley, and M. Kraft. First-principles thermochemistry for the combustion of TiCl_4 in a methane flame. *Proceedings of the Combustion Institute*, 33(1):493–500, 2011. doi:10.1016/j.proci.2010.05.011.
- [51] W. Tsang. Chemical Kinetic Data Base for Combustion Chemistry. Part 2. Methanol. *Journal of Physical and Chemical Reference Data*, 16(3):471–508, 1987. doi:10.1063/1.555802.
- [52] H.-J. Werner, P. J. Knowles, G. Knizia, F. R. Manby, M. Schütz, et al. Molpro, version 2012.1, a package of ab initio programs, 2012. see, <http://www.molpro.net>.
- [53] R. West, R. Shirley, M. Kraft, F. C. Goldsmith, and W. H. Green. A detailed kinetic model for combustion synthesis of titania from TiCl_4 . *Combustion and Flame*, 156(9):1764–1770, 2009. doi:10.1016/j.combustflame.2009.04.011.